Journal of Applied Physics

RESEARCH ARTICLE | APRIL 04 2024

Oxide dissolution and oxygen diffusion scenarios in niobium and implications on the Bean–Livingston barrier in superconducting cavities

E. M. Lechner ; J. W. Angle ; A. D. Palczewski ; F. A. Stevie ; M. J. Kelley ; C. E. Reece

J. Appl. Phys. 135, 133902 (2024)
https://doi.org/10.1063/5.0191234
CHORUS

Journal of Applied Physics ARTICLE pubs.aip.org/aip/jap

Oxide dissolution and oxygen diffusion scenarios in niobium and implications on the Bean–Livingston barrier in superconducting cavities

Cite as: J. Appl. Phys. **135**, 133902 (2024); doi: 10.1063/5.0191234
Submitted: 12 December 2023 · Accepted: 9 March 2024 ·
Published Online: 4 April 2024

E. M. Lechner,[1,a)] J. W. Angle,[2] A. D. Palczewski,[1] F. A. Stevie,[3] M. J. Kelley,[1,4] and C. E. Reece[1]

AFFILIATIONS

[1]Thomas Jefferson National Accelerator Facility, Newport News, Virginia 23606, USA
[2]Nanoscale Characterization and Fabrication Laboratory, Virginia Polytechnic Institute and State University, Blacksburg, Virginia 24060, USA
[3]Analytical Instrumentation Facility, North Carolina State University, Raleigh, North Carolina 27695, USA
[4]Virginia Polytechnic Institute and State University, Blacksburg, Virginia 24060, USA

[a)]**Author to whom correspondence should be addressed:** lechner@jlab.org

ABSTRACT

We generalize a native Nb_2O_5 dissolution model [G. Ciovati, Appl. Phys. Lett. **89**, 022507 (2006)] to sequential overlayer dissolutions, multilayer dissolution, and realistic temperature profiles, which may be applicable to other materials. The model is applied to secondary ion mass spectrometry depth profile measurements for varying temperature profiles and two-step oxide dissolution in Nb and found to agree well. In the context of the Meissner screening response due to impurity profiles on the length scale of the London penetration depth, the shallow diffusion of O impurities results in a substantial decrease in the peak supercurrent density near the surface. In this framework, oxide dissolution and oxygen diffusion can account for a rise in peak supportable magnetic field in SRF cavities with baking time and a suppression after the optimal baking time is reached, in good agreement with peak-field baking temperatures and times as well as recent quench field measurements.

I. INTRODUCTION

Reliably tuning the electron mean free path, l, in superconducting devices via surface impurity alloying can enhance their performance.[1–7] These applications include superconducting radio frequency (SRF) cavities,[8,9] superconducting qubits,[10] microwave detectors,[11] as well as many others. In superconducting resonators, the effect of increasing impurity content on the surface resistance, R_s, is due to the competition between the diminishing dissipative conductivity, $\sigma_1(l)$, and the expanding London penetration depth, $\lambda(l)$. An optimal competition between these two for $R_s \propto \sigma_1\lambda^3$ leads to a minimum at $l \approx \xi_0/2$, where ξ_0 is the superconductor's coherence length.[3]

Major particle accelerator projects use or plan to utilize SRF technology to facilitate fundamental research.[12–23] In such projects, trace impurities have tremendous impact on improving superconducting cavity performance.[8,24,25] Nb superconducting radio frequency cavities alloyed with nitrogen,[8,9] titanium,[26,27] or other impurities[28] have yielded significant reductions of the BCS surface resistance. This advantage is being exploited by the LCLS-II and LCLS-II HE projects[29,30] by using N-alloyed Nb in their continuous wave accelerators. Recently, it has been shown that a native oxide dissolution and oxygen diffusion process is responsible for the increase in quality factor in SRF cavities.[31–33] The Nb–O solid solution is composed of O dissolved in octahedral interstices,[34] which alter the physical and electronic properties of Nb.[34–37] Elevated O concentration in Nb is associated with decreases in T_c, B_c, and B_{c1} but enhancements in κ, B_{c2}, and B_{c3}.[35,38] The presence of O may help prevent precipitation of deleterious phases like hydrides.[39–41] Generalizations of the Nb pentoxide dissolution and oxygen diffusion model described by

Ciovati for Nb[42] could be applied to other materials like Zr[43] or Ta,[44] a material considered for superconducting qubits, to enhance the low field surface resistance and increase qubit coherence times.[45,46]

Preservation of the Meissner state is imperative for low-loss, high accelerating field SRF cavity performance. The Bean–Livingston barrier[47] preserves the Meissner state above B_{c1}, where it is metastable, up to the superheating field, B_{sh}. At B_{sh}, the surface is absolutely unstable to vortex nucleation, allowing penetration of highly dissipative vortices that may trigger thermal instabilities.[48,49] Through surface engineering it is expected that B_{sh} can be extended beyond the substrate's intrinsic limit. Either by a controlled impurity profile[1,50] or by a dirty Nb layer directly coupled to a clean Nb substrate or separated by an insulator.[2,51] A goal remains to develop impurity diffusion models to tune interstitials optimally to modify R_s and E_{acc} for an intended application. This work requires the use of secondary ion mass spectrometry (SIMS) because of its high depth resolution and ability to quantify trace impurities.

In this work, we extend the thin overlayer dissolution model to sequential overlayer dissolutions, multilayer dissolution, and realistic temperature profiles. The model is compared with SIMS depth profiles for sequential oxide dissolutions and realistic temperature profiles. We apply this model to the case of shallow migration of O in Nb and examine its expected effect on near-surface supercurrent density.

II. EXPERIMENTAL

SIMS measurements were made using a CAMECA 7f Geo magnetic sector SIMS instrument on Nb samples as described elsewhere.[31,52,53] A Cs^+ primary ion beam accelerated to 5 keV was used to impact the samples biased at −3 kV, yielding an impact energy of 8 keV. The Cs^+ ion beam was rastered over an area of $150 \times 150\,\mu m^2$ with the collected data coming from a $63 \times 63\,\mu m^2$ area in the center of the larger raster. Quantitation of the SIMS oxygen depth profiles was made using an implant standard to convert the ion signal to impurity concentration. Here, we used an O implant standard dosed with O at 2×10^{15} atoms/cm^2 at 180 keV by Leonard Kroko Inc. to quantify the O composition of the RF penetration layer and beyond by detecting $^{16}O^-$ in conjunction with a $^{93}Nb^-$ reference signal.

III. OXIDE DISSOLUTION AND OXYGEN DIFFUSION

A thin overlayer decomposition and diffusion model has been proposed by Ciovati[42] to describe the decomposition of Nb_2O_5 and O diffusion in the Nb_2O_5/Nb system to describe the migration of O in Nb during heat treatments between 100 and 200 °C. Ciovati's model considers one-dimensional O diffusion from an initial interstitial oxygen concentration present at the oxide/metal interface and diffusion of oxygen from thermal decomposition of an oxide overlayer. Recently, vacuum heat-treated Nb measured by secondary ion mass spectrometry found oxygen diffusion profiles consistent with Ciovati's model.[31] We extend this model to multistep dissolutions, multilayers, and temperature profiles relevant to real furnaces.

Impurity diffusion through a multilayer system like an oxide is inherently complex and results in the need for several boundary conditions for the impurity concentration. Here, we consider irreversible decomposition in the thin layer limit where mass transport through the oxide does not delay the availability of the impurity to the substrate. This is a serviceable approximation when the diffusion lengths within the oxides are much greater than the oxide thicknesses. In the case of Nb, the migration of O through Nb_2O_5 oxide may be slow.[54] The approximation presented here may lose accuracy for short vacuum heat treatment times or low temperatures if impurity migration through the oxides is expected to be a principal component of the impurity content in the substrate. The decomposition of the native Nb oxide can be modeled by two consecutive irreversible reactions each releasing interstitial O free to migrate toward the bulk,[55]

$$Nb_2O_5 \xrightarrow{k_1} 2NbO_2 + O \xrightarrow{k_2} 2NbO + 3O. \tag{1}$$

Nb_2O_5, NbO_2, and NbO are represented by reactants A, B, and C, respectively, and the rate equations for these reactions are as follows:

$$-\frac{dA}{dt} = k_1 A;\ -\frac{dB}{dt} = k_2 B - 2k_1 A;\ -\frac{dC}{dt} = -k_2 B, \tag{2}$$

and the isothermal solutions are as follows:

$$\begin{aligned} A &= A_0 \exp(-k_1 t), \\ B &= (2A_0 k_1(\exp(-k_1 t) - \exp(-k_2 t)))/(k_2 - k_1) \\ &\quad + B_0 \exp(-k_2 t), \\ C &= 2A_0((k_1 \exp(-k_2 t) - k_2 \exp(-k_1 t))/(k_2 - k_1) + 1) \\ &\quad + B_0(1 - \exp(-k_2 t)) + C_0, \end{aligned} \tag{3}$$

where X_0 is the initial concentration of the reactant. The impurity source term located at the overlayer position, $x = a_n$, is related to the rate of the production of reactant B from A's dissolution by

$$k_1 A \propto q_1(t) = u_0 k_1 \exp(-k_1 t)\delta(x - a_n) = \gamma_1(t)\delta(x - a_n), \tag{4}$$

and the rate of production of NbO is similarly proportional to production of C,

$$\begin{aligned} k_2 B \propto q_2(t) = \Big(&\frac{2u_0 k_1 k_2}{k_2 - k_1}(\exp(-k_1 t) - \exp(-k_2 t) \\ &+ u_1 k_2 \exp(-k_2 t))\Big)\delta(x - a_n) = \gamma_2(t)\delta(x - a_n). \end{aligned} \tag{5}$$

These equations can be easily extended to N-sequential irreversible dissolution steps following the same procedure that only changes the form of $\gamma_N(t)$.

The diffusion of oxygen released by oxide dissolution is modeled using the one-dimensional Fick's second law with finite sources in a semi-infinite slab of metal existing at $x \geq 0$ in the

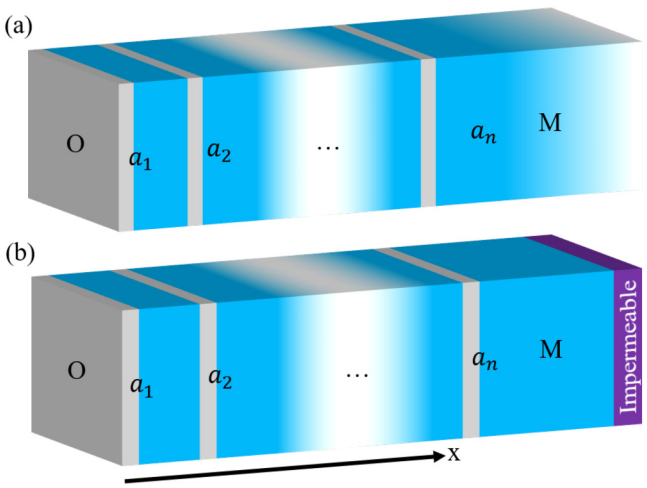

FIG. 1. (a) Semi-infinite slab geometry and (b) thin film on O-impermeable substrate. O(gray layers) indicates dissolvable oxides located at a_n and M(blue layers) denotes the substrate absorbing the mobile species produced from overlayer dissolution.

geometry shown in Fig. 1(a),

$$\frac{\partial c(x,t)}{\partial t} = D(T)\frac{\partial c(x,t)}{\partial x^2} + \sum_X q_X(x,t), \tag{6}$$

where c is the concentration of the impurity and D is the diffusion coefficient. The diffusion coefficients and rate constants associated with arbitrary component, X, dissolution are assumed to exhibit Arrhenius behavior such that $k_X(T) = A_X\exp(-E_{a_X}/RT)$ and $D(T) = D_0\exp(-E_{a_D}/RT)$. We use the method of reflection and superposition[56] to construct a solution that preserves boundary conditions for the semi-infinite slab with impurity sources located at a_n, and the diffusion equation becomes

$$\frac{\partial c(x,t)}{\partial t} - D(T)\frac{\partial c(x,t)}{\partial x^2} = \sum_{n=1}^{m}\gamma_n(t)(\delta(x+a_n)+\delta(x-a_n)), \tag{7}$$

where $\gamma_n(t) = \sum_X \gamma_{nX}(t)$. The diffusion equation is solved via Fourier transform with an initial impurity concentration residing at the oxide/metal interface, $c(x,0) = \nu_n\delta(x-a_n)$, which yields

$$c(x,t) = \sum_{n=1}^{m}\frac{\nu_n}{\sqrt{4\pi Dt}}\left(\exp\left(-\frac{(x-a_n)^2}{4Dt}\right)+\exp\left(-\frac{(x+a_n)^2}{4Dt}\right)\right) + \int_0^t \frac{\gamma_n(s)}{4\pi D(t-s)}\left(\exp\left(-\frac{(x-a_n)^2}{4D(t-s)}\right)+\exp\left(-\frac{(x+a_n)^2}{4D(t-s)}\right)\right)ds + c_\infty. \tag{8}$$

For a constant-temperature irreversible process, γ_n is only dependent on time, which allows Eq. (8) to hold for any number of component dissolutions. As an example, considering only the Nb_2O_5 dissolution parameters determined in Ref. 31, Eq. (8) is plotted in Fig. 2(a) for $T = 280°C$. Equation (8) reduces to Ciovati's equation and Eq. (9) for a superficial oxide dissolution and diffusion process with negligible background concentration of O and negligible NbO_2 dissolution,[42]

$$c(x,t) = \frac{\nu_0}{\sqrt{\pi Dt}}\exp(-x^2/4Dt) + \int_0^t \frac{u_1k_1\exp(-k_1t)}{\sqrt{\pi D(t-s)}}\exp(-x^2/4D(t-s))ds. \tag{9}$$

Using Eq. (9) with the contributions from Nb_2O_5 and NbO_2 dissolution source terms, we have attempted to fit the SIMS measurements in our previous work.[31] The fit to that data did not yield NbO_2 dissolution parameters to any reasonable confidence, and results are not presented here. We suspect that a reasonable extraction of dissolution parameters will require a deeper exploration of the heat treatment time and temperature parameter space and hinge on high-quality SIMS measurements on single crystals to combat the effects of ion channeling.[53] For higher temperatures and longer vacuum heat treatment times, the effects of NbO_2 dissolution will become relevant depending on the nature of the decomposition,[55] where the NbO_2 layer has been shown to dissolve after Nb_2O_5 dissolution.[57,58]

Equation (6) may be applied to an engineered multi-layer surface containing an impurity impermeable layer (impurity diffusion barrier) at $x = d$. This imposes the boundary condition $\partial_x c(d,t) = 0$. This geometry is shown in Fig. 1(b). Through the method of reflection and superposition[56] to preserve the boundary conditions of the system, the source positions must be modified to

$$\frac{\partial c}{\partial t} - D\frac{\partial c}{\partial x^2} = \sum_{k=-\infty}^{\infty}\sum_{n=1}^{m}\gamma_n(\delta(x+a_n-2kd)+\delta(x-a_n-2kd)), \tag{10}$$

and the solution, made by Fourier transform, is

$$c(x,t) = \sum_{k=-\infty}^{\infty}\sum_{n=1}^{m}\frac{\nu_n}{\sqrt{4\pi Dt}}\left(\exp\left(-\frac{(x-a_n-2kd)^2}{4Dt}\right)+\exp\left(-\frac{(x+a_n-2kd)^2}{4Dt}\right)\right) + \int_0^t\frac{\gamma_n(s)}{4\pi D(t-s)}\left(\exp\left(-\frac{(x-a_n-2kd)^2}{4D(t-s)}\right)+\exp\left(-\frac{(x+a_n-2kd)^2}{4D(t-s)}\right)\right)ds + c_\infty. \tag{11}$$

In Figs. 2(a) and 2(b), the semi-infinite layer dissolution and finite thickness diffusion model is compared using Nb_2O_5 decomposition and O diffusion parameters determined from a previous study[31] and are listed in Table I. It should be noted that the values of the O diffusion parameters, D_0 and E_{aD}, are higher than that typically reported by internal friction measurements.[59] It is known that the presence of other impurities can substantially increase the

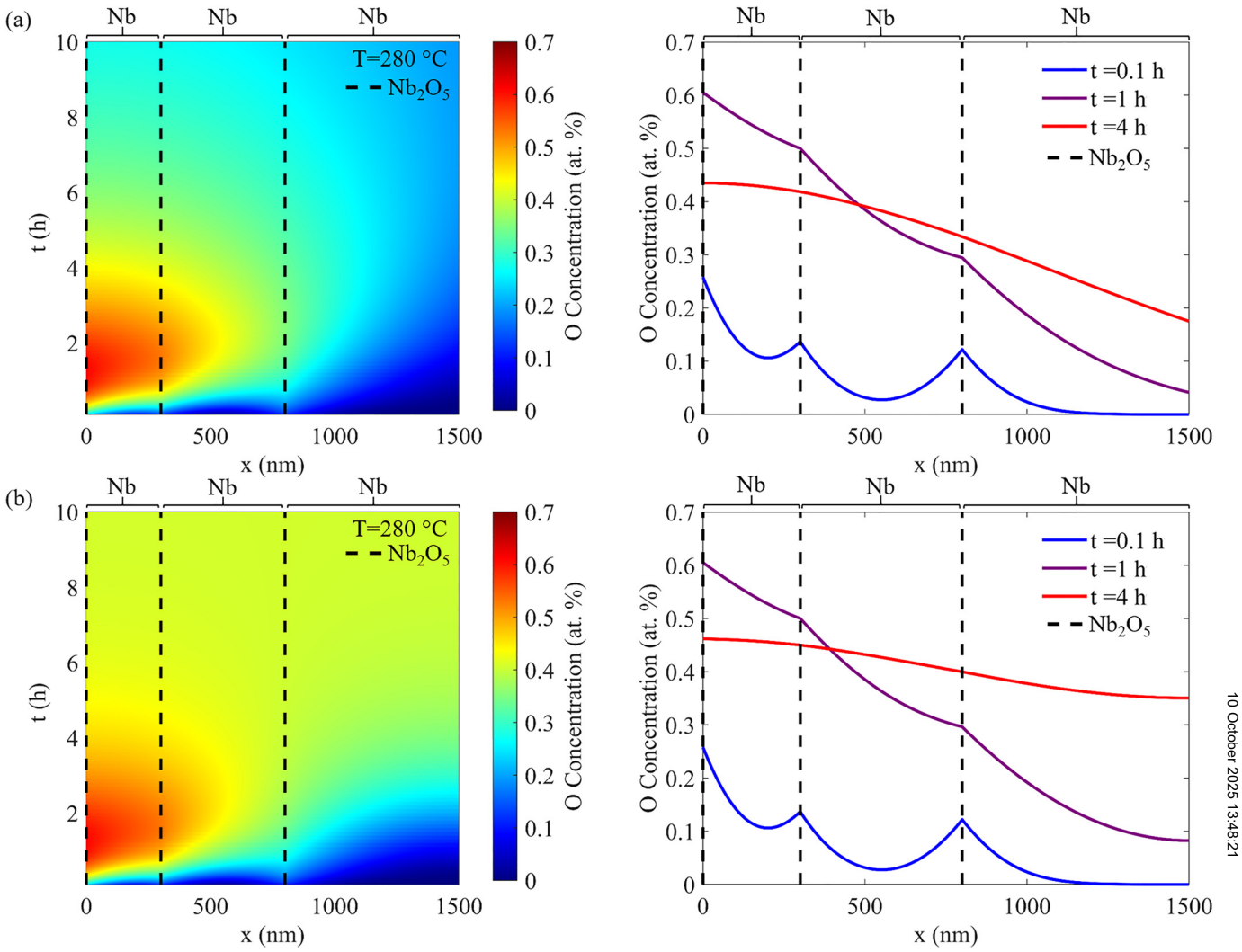

FIG. 2. Comparison of the semi-infinite and finite-thickness-impermeable-substrate solution to the diffusion equations using dissolution and diffusion parameters described from Ref. 31 at T = 280°C. (a) Colorplot and concentration profiles of the semi-infinite slab solution and concentration profiles at selected times. (b) Colorplot and concentration profiles of the finite-thickness-impermeable-substrate solution and concentration profiles at selected times. Black vertical dashed lines indicate the location of the sources (Nb_2O_5 layers) at x = 0, 300, and 800 nm. All thin oxide layers modeled are equal in O content.

activation energy of O diffusion[34,60] and can be affected by strain. Regardless, the direct, near-surface O diffusion coefficient, *D*, in SRF-grade Nb measured by Lechner *et al.* generally agrees within a factor of ∼ 2 of other indirect estimations,[60–62] in the temperature range of 140–350°C.

The finite-thickness-impermeable-substrate model may be realized by multilayer Nb films deposited on an oxygen diffusion barrier material like MgO, Si, Al_2O_3, or AlN[63–69] at temperatures low enough to preserve the native Nb oxide and then allow the newly deposited Nb surface to oxidize. In context of SIMS measurements, an impermeable substrate geometry could allow for precise determinations of oxide decomposition and O diffusion in Nb for native oxide or anodized Nb[70,71] dissolution without lengthy secondary ion mass spectrometry measurements by only needing to depth profile to the impermeable substrate. The applicability of this structure to superconducting RF structures may allow thorough explorations of preservation of the Bean–Livingston barrier by introducing a dirty layer on top of a clean Nb substrate as described by Kubo,[2] but care must be taken not to introduce too much oxygen during dissolution as many superconducting properties can be degraded.[35,72]

In practice, the time heating to temperature and cooling down in furnaces can be substantial. These effects should be considered when attempting to precisely engineer impurity profiles on the

TABLE I. Model parameters used for theoretical O concentration profiles in Figs. 3 and 4.

	Ref. 31	NL298	NL321	NL324	NL563	NL564
u_0 (at. % nm)	200	200	257	187	155	138
v_0 (at. % nm)	3.5	3.5	3.5	3.5	3.5	13
$A \times 10^9$ (1/s)	0.9	0.994	0.959	0.993	0.986	0.993
E_a (kJ/mol)	131	132	134	135	137	135
D_0 (cm^2/s)	0.075	0.077	0.067	0.073	0.059	0.065
E_{aD} (kJ/mol)	119.9	118	120	119	118	119

length scale of the London penetration depth to engage with modern theories of superheating field enhancement.[1,2,50,73] To model an arbitrary temperature profile of a real furnace for the Nb_2O_5 oxide dissolution, we employ the one-dimensional Fick's second law with a time-dependent temperature,

$$\frac{\partial c(x,t)}{\partial t} = D(T(t))\frac{\partial c(x,t)}{\partial x^2} + q(t, T(t)). \tag{12}$$

The initial concentration of oxygen at the oxide/metal interface is given by $c(x, 0) = v_0\delta(x)$. Starting from the rate equation of oxide dissolution, the O source is related to rate equation by

$$-\frac{dA}{dt} \propto q = u_0 k(T(t)) \exp\left(-\int_0^t k(T(s))ds\right)\delta(x). \tag{13}$$

The Fick's law diffusion equation is subjected to the boundary conditions $c(x = \infty) = c_\infty$ and $c'(x = \infty) = 0$. To test the model, three samples were vacuum heat treated with a ramp rate of 1°C/min to a maximum temperature and then allowed the cool. The temperature of the samples was measured with a thermocouple, while the furnace temperature was regulated by monitoring the furnace hot zone wall. A ramp-up/ramp-down profile was chosen to showcase the role of oxide dissolution and migration, which may be relevant for short heat treatments where these processes contribute significantly. Sample temperature measurements during vacuum heat treatment are shown in Fig. 3(a). SIMS depth profiles of those samples are shown in Fig. 3(b). To isolate the interstitial O component and remove any possible influence from the high oxygen content oxide, SIMS depth profiles start at ~ 25 nm. The calculations in Fig. 3(b) were made using MATLAB to numerically solve Eq. (12) using the source term from Eq. (13) using the temperature profiles in Fig. 3(a). The parameters used for the calculations are presented in Table I. The largest variation in parameters for the theoretical O concentration profiles are from the oxide source term and diffusion coefficient.

A two-step impurity alloying process may be advantageous for SRF cavity performance to first establish a background concentration and then introduce a shallow impurity profile for enhancing peak magnetic field. Sequential heat treatments after reoxidation can be modeled by evaluating the first alloying step using Eq. (8), then using that as the initial condition for the following step evolved numerically under Eq. (7) using a replenished source. Figure 4 shows modeling of samples vacuum heat treated, oxidized, and vacuum heat treated again. The parameters used for the modeling are listed in Table I.

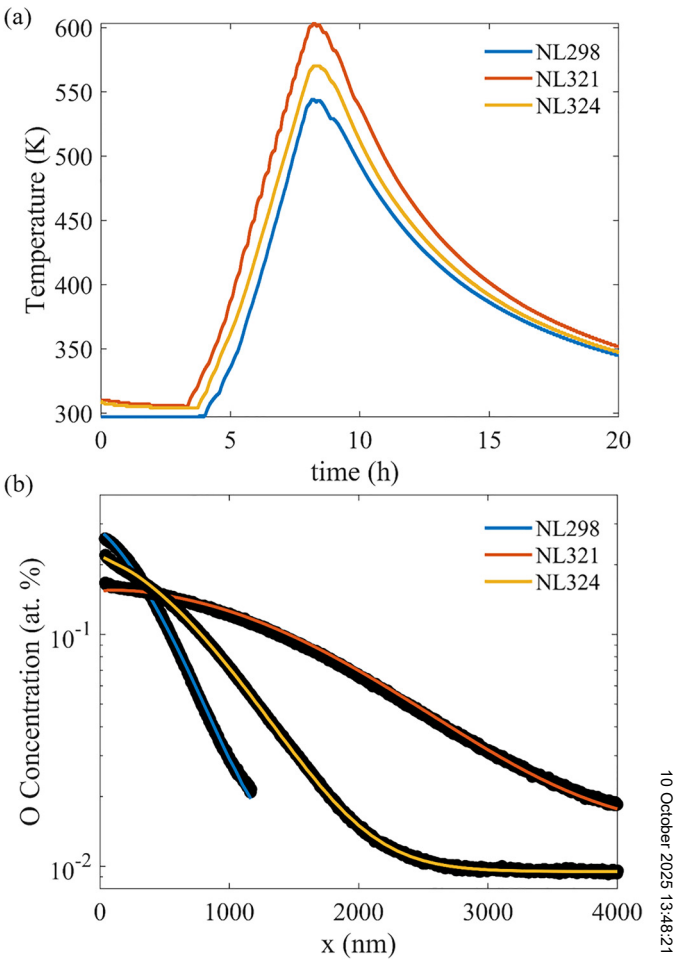

FIG. 3. (a) 1°C/min ramp up and ramp down temperature profiles that samples were subjected to. (b) SIMS depth profiles (black circles) of the samples and their theoretical fits (colored lines) as described in the text and using the temperature profiles in (a) within the calculation.

As shown in Table I, there is some spread in oxide dissolution and O diffusion parameters of fits to the diffusion model in limits not previously explored. The O diffusion parameters E_{aD} and D_0 are generally consistent with the previous exploration.[31] Examining $D(T)$ extracted from these single curve fits at the extremes, at 100°C, D has an average diffusion coefficient of $1.6 \pm 0.5 \times 10^{-18}$ and $7.4 \pm 1.6 \times 10^{-16}$ cm^2/s at 350 °C. For, u_0, the parameter quantifying the amount of dissolvable Nb_2O_5, we find 190 ± 40 at. % nm suggesting that the magnitude of O content can be determined to be ±20%. There may be a decrease in u_0 in the two-step baked samples due to a thinner Nb_2O_5 in the mid-T baked type samples.[74] While these parameters are generally within the deviations expected from RSF variation on polycrystalline Nb, real differences in oxide thickness and composition before dissolution

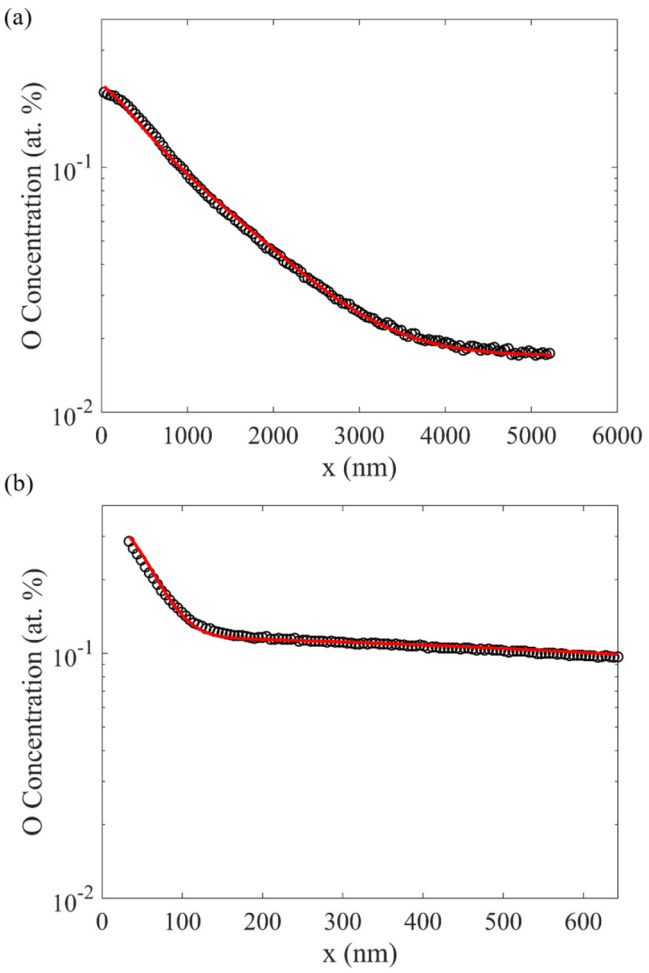

FIG. 4. SIMS depth profiles (black circles) of Nb samples first-step vacuum heat treated at 300 °C for 2.5 h, reoxidized, and then second-step vacuum heat treated. (a) NL563 received a second-step 250 °C vacuum heat treated for 3 h (b) NL564 received a second-step 120 °C vacuum heat treatment for 72 h. The red lines are the theoretical fits using oxide dissolution and oxygen diffusion parameters as described in Table I.

could be a compounding factor to the spread. Determination of ν_0 is only possible for baking temperatures where oxide dissolution is not dominant. Determination of ν_0 was only possible for NL564. It was found that ν_0 was much larger than previously observed.[31] We speculate that the enhanced interstitial O concentration may be due to the fact that this oxide was grown in air, in contrast to previously investigated samples.[31] The oxide dissolution parameters E_a and A are consistent with previous estimations.

IV. IMPLICATIONS FOR SUPERCONDUCTING DEVICES

High-field Q-slope (HFQS) is a phenomenon characterized by a rapid decay of the quality factor, Q_0, above accelerating gradients between 20 and 30 MV/m, which is preceded by a slower decay in Q_0 below the onset of HFQS.[75] The amelioration of this effect on electropolished Nb surfaces has involved "low-temperature baking" consisting of vacuum heat treatment at temperatures between 110 and 160 °C for several hours, e.g., 120 °C for 48 h.[75] Recent theories of extending the peak magnetic fields in SRF cavities have focused around reducing the peak current density near the surface to preserve the Bean–Livingston barrier. Guarding the Bean–Livingston barrier with impurity profiles or a "dirty" surface bilayer[1,2,50,73] extends the peak magnetic field before the metastable Meissner state becomes absolutely unstable to vortex penetration.[48,51]

Key works in understanding the effects associated with low temperature baked Nb superconducting radio frequency cavities identified that the amelioration of HFQS in Nb cavities is related to a decrease in the electron mean free path[75] and the reappearance of HFQS after subjecting a low temperature baked cavity to nanometer-scale chemical removal.[76–78] Recent re-analysis[79] of low-energy muon spin rotation measurements on low-temperature baked Nb indicate that strong changes in the Meissner screening profile[80] do not exist, allowing for the possibility of a smoothly varying Meissner screening profile. It has been speculated for some time that the HFQS ameliorating vacuum heat treatment may be related to oxygen diffusion in some way.[81–83] Recent evidence has been provided that an impurity profile may play a role in HFQS amelioration in "N-infused" cavities.[73] The spatial distribution of the magnetic field and supercurrent density can be described by the one-dimensional London equation for a spatially inhomogeneous London penetration depth. This equation naturally arises from the application of Faraday's law of induction on the London equation, which describes the response of the supercurrent density to electric fields,[84,85]

$$\lambda(x)^2 B'' + 2\lambda(x)\lambda'(x)B' = B. \tag{14}$$

For O in Nb, the change in the mean free path can be estimated from the change in resistivity,[86]

$$l(x) = \frac{\sigma}{\Delta\rho_O}, \tag{15}$$

where $\sigma = 0.37 \times 10^{-15}\Omega\,\mathrm{m}^2$[37] and $\Delta\rho_O(x) = ac(x)$, where c is the percent concentration of O and $a = 4.5 \times 10^{-8}\Omega\,\mathrm{m}$.[87] The spatially dependent London penetration depth is assumed to be local and estimated according to the following expression:[88]

$$\lambda(x) = \lambda_0\sqrt{1 + \xi_0/l(x)}. \tag{16}$$

Here, the clean limit of the London penetration depth $\lambda_0 = 39$ nm and coherence length $\xi_0 = 38$ nm.[89] A small increase in λ by $\sim 10\%$ from the nonlinear Meissner effect is neglected.[90] With these estimations, Eq. (14) can be calculated for different temperature and times for the heat treatment process using the oxide dissolution and O diffusion model described in Ref. 31. Figure 5 shows the normalized magnetic field, supercurrent density, and oxygen impurity profile at different temperatures and times of heat treatment. There is a small widening of the Meissner screening profile, B/B_0. Such a small change in Meissner screening profile may be observable in muon spin rotation experiments but may be difficult to distinguish.[79] The supercurrent density was

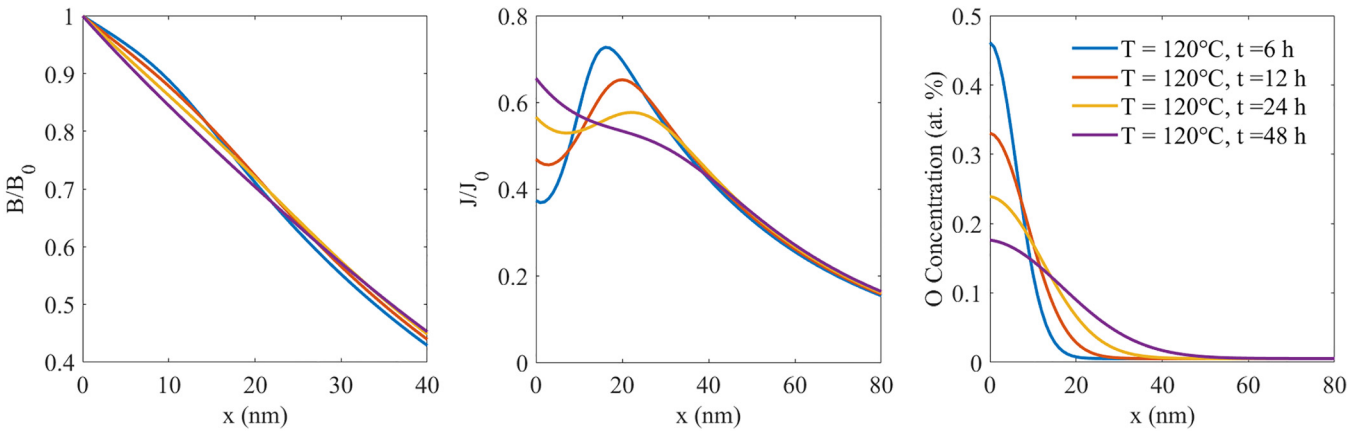

FIG. 5. Normalized magnetic field, supercurrent density, and O impurity distributions predicted for various times at T = 120°C.

calculated using $\nabla \times \mathbf{B} = \mu_0 \mathbf{J}$. Starting with short baking times at 120 °C, the supercurrent density is deformed from its exponential form and shifted away from the surface. With longer baking times, the peak supercurrent density extends further from the surface and is suppressed until the spatial distribution of the impurity profile is uniform enough to start returning to its exponential nature. The ratio, $J_{\max 0}/\max(J(x, T, t))$, of peak supercurrent density of clean Nb, $J_{\max 0}$, to the maximum spatial supercurrent density, $\max(J(x, T, t))$, in the O-alloyed Nb represents the factor of peak field enhancement before the depairing current density of the clean limit is reached in O-alloyed Nb. This ratio can be mapped out in the O-alloying $T - t$ space as shown in Fig. 6. There exists a ridge of heat treatment times and temperatures that minimize the peak spatial supercurrent density with respect to the clean case. Despite slightly enhanced O concentration near the surface for higher temperature processes, this ridge in $T - t$ space shows no significant difference as a function of temperature. This invariance is due to the form of Eq. (16) where the penetration depth would change negligibly with a small increase in O from oxide dissolution. Furthermore, the ridge is consistent with the temperatures and times where efficacy for HFQS amelioration has been shown in previous works for low temperature baking at different temperatures.[91–94] Notably, the model predicts that the 120 °C for 48 h recipe may not ideally minimize the spatial distribution of the supercurrent density and an ideal baking time may be more consistent with the 120 °C for 24 h. It should be noted that the proposed mechanism of high-field Q-slope amelioration described here is much different from that of Ref. 42, which proposed that the effect is due to a minimization of O near the surface upon heat treatment for some time. This scenario was explicitly ruled out.[95]

Recently, insightful measurements by Bafia *et al.*[96] clearly showed a rise and gentle decay of the quench field, E_q, with baking time and that cavities baked at different temperatures tend to fall on a universal line when scaled with oxygen diffusion depth using the model of Ref. 97. These observations are consistent with the model of high-field Q-slope amelioration proposed here. Since the quench fields (peak magnetic fields, B_p) are essentially unaffected by baking temperature, we can rescale the O-diffusion depth in Fig. 5 of Ref. 96 to effective baking times at 120 °C, as shown in Fig. 7. The peak field should scale as $E_q = E_{q0} J_{\max 0}/\max(J(x, T, t))$. A best fit of this model, plotted in red in Fig. 7, using the oxide dissolution and oxygen diffusion parameters of Lechner *et al.*[31] and allowing the interstitial O content v_0 and E_{q0} to vary, we find $E_{q0} = 29.2 \pm 0.5$ MV/m and $v_0 = 2.6 \pm 0.3$ at. % nm, close to the value of 3.5 at. % nm extracted in Lechner *et al.*[31] Using $E_{q0} = 29.2$ MV/m (B_p = 124 mT) and the parameters extracted in Lechner *et al.*, an optimal treatment is estimated to produce ∼ 50 MV/m (B_p = 212 mT) TESLA-shaped cavities[98] as shown in the blue dashed line in Fig. 7.

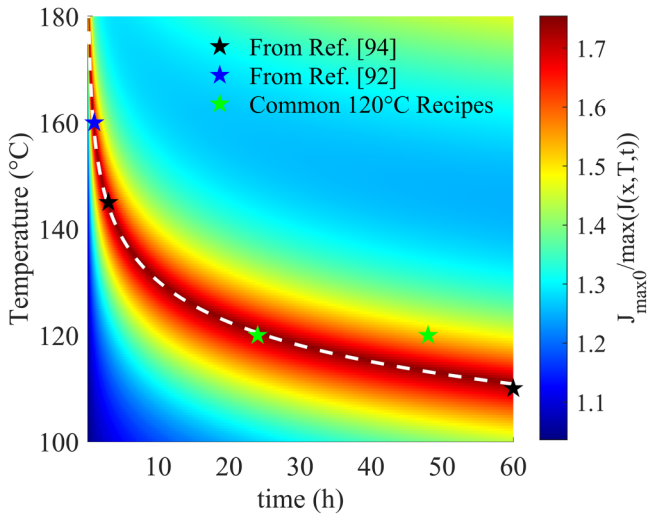

FIG. 6. (a) $T - t - J_{\max 0}/\max(J(x, T, t))$ colormap showing the existence of a ridge of optimal baking times and temperatures to reduce the peak supercurrent compared to the clean case, $J_{\max 0}/\max(J(x, T, t))$. The white dashed line follows the path of minimized peak supercurrent density.

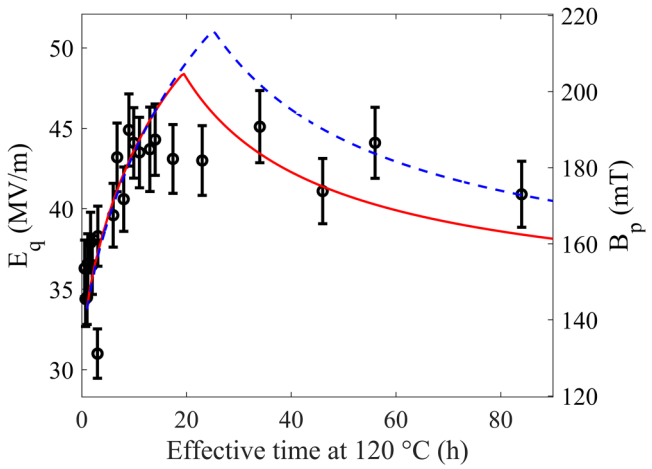

FIG. 7. Rescaled data of Bafia *et al.*[96] to effective 120 °C baking time (black circles), best fit to $E_q = E_{q0} J_{max\,0} / \max(J(x, T, t))$ (solid red line) and prediction of $E_q = E_{q0} J_{max\,0} / \max(J(x, T, t))$ using the parameters from Ref. 31 (dashed blue line).

Between ∼ 100 and 200 °C, O diffusion is dominated by the migration of interstitial O located near the oxide/metal interface, quantified by ν_0. The peak supercurrent density can be suppressed by loading the surface with a greater concentration of impurities, which enlarges the London penetration depth. This enhanced O concentration must be spread further by diffusion. The enhancement of peak field in the blue dashed line of Fig. 7 as compared with the red line is due to the larger O concentration of $\nu_0 = 3.5$ at. % nm as compared with $\nu_0 = 2.6$ at. % nm. Naturally, optimal bake times will scale with the diffusion coefficient, D.

The analysis presented here shows that Bean–Livingston barrier preservation via oxygen diffusion is capable of capturing the increase and decrease in quench field with vacuum heat treatment time. In this framework, what could be the role of nano-hydride precipitates? It is known that severe plastic deformation occurs in Nb affected by Q-disease, which may facilitate Bean–Livingston breakdown well below its theoretical maximum[99,100] topographically[101–106] or facilitate vortex entry through weakened superconductivity or proximity effect.[107] We suggest that nano-hydride precipitation may be more involved in setting $E_{q0}(B_{p0})$, while the extension of $E_q(B_p)$ with low-temperature vacuum annealing is related to prevention of vortex entry of the imperfect surface. Recent calculations show that vortex nucleation and dissipation through hydrides may be especially lossy and bring about high-field Q-slope.[108]

V. CONCLUSIONS

We further developed a model of overlayer dissolution and diffusion potentially relevant for a variety of materials with a dissolving overlayer. The model has been extended to consecutive irreversible reactions, multilayers, varying temperature, sequential dissolution, and films on impermeable substrates. These methods may be useful in guiding heat treatments toward tailored O content deep in to the substrate where a single native oxide dissolution would be insufficient. In particular, varying O diffusion depths at a constant elevated O content near the surface may provide insight into the effectiveness of hydride blocking by O.[108] The model was compared to SIMS O concentration depth profiles and shows promise but will require a dataset spanning larger portions of the $T - t$ space to determine parameters related to NbO_2 dissolution. This in-depth investigation of the native oxide dissolution and O diffusion process using single crystals is a topic of future study.

It was shown that optimal low-temperature baking times and temperatures scale with oxygen diffusion parameters[81–83] because the oxygen impurities bend the supercurrent. An optimal nanostructuring of the surface with O requires that the O impurities extend over a length scale set by the London penetration depth. The models of oxygen diffusion and supercurrent density deformation described here also provide insight into other optimal baking temperatures and times that have been previously explored in literature. This reduction in the peak supercurrent density also explains the rise and reduction of the onset of quench fields with greater baking times observed by Bafia *et al.*[96] Beside superconducting RF cavities, this process should be applicable to devices. While the modified London equation is oversimplified for O-alloyed Nb, quasi-classical theories of superconductivity[1] that consider the modification of superconducting parameters with O content[35,36] will provide more accurate predictions.

Beyond the impurity alloying described here, the oxide dissolution process may provide an opportunity to modify the metallic oxide on the surface. Tuning the thickness of the overlayer and its contact resistance may have a considerable impact on deforming the quasi-particle density of states toward enhancing quality factors that improve energy efficiency of particle accelerator applications.[6,7,109] Alternatively, a metallic oxide could be formed on the surface by dissolving both the NbO_2 and Nb_2O_5 and then preserved by capping the surface with a robust insulating O diffusion barrier.

ACKNOWLEDGMENTS

This material is based upon work supported by the U.S. Department of Energy, Office of Science, Office of Nuclear Physics under contract DE-AC05-06OR23177, including supplemental funding by the Office of Science, Office of Nuclear Physics Early Career Award to A. D. Palczewski. J. W. Angle was supported by the U.S. Department of Energy, Office of Science, Office of High Energy Physics under Grant No. DE-SC-0018918 to Virginia Polytechnic Institute and State University. We gratefully acknowledge C. Baxley, R. Overton, and T. Harris for support in sample preparation.

AUTHOR DECLARATIONS

Conflict of Interest

The authors have no conflicts to disclose.

Author Contributions

E. M. Lechner: Conceptualization (lead); Data curation (equal); Formal analysis (lead); Software (lead); Writing – original draft

(lead); Writing – review & editing (lead). **J. W. Angle:** Data curation (equal); Formal analysis (supporting); Writing – original draft (supporting); Writing – review & editing (supporting). **A. D. Palczewski:** Funding acquisition (equal); Supervision (supporting); Writing – review & editing (supporting). **F. A. Stevie:** Supervision (supporting); Writing – review & editing (supporting). **M. J. Kelley:** Conceptualization (supporting); Funding acquisition (equal); Supervision (equal); Writing – review & editing (supporting). **C. E. Reece:** Conceptualization (supporting); Funding acquisition (equal); Supervision (equal); Writing – review & editing (supporting).

DATA AVAILABILITY

The data that support the findings of this study are available from the corresponding author upon reasonable request.

REFERENCES

[1]V. Ngampruetikorn and J. A. Sauls, "Effect of inhomogeneous surface disorder on the superheating field of superconducting RF cavities," Phys. Rev. Res. **1**, 012015 (2019).

[2]T. Kubo, "Superheating fields of semi-infinite superconductors and layered superconductors in the diffusive limit: Structural optimization based on the microscopic theory," Supercond. Sci. Technol. **34**, 045006 (2021).

[3]T. Kubo, "Effects of nonmagnetic impurities and subgap states on the kinetic inductance, complex conductivity, quality factor, and depairing current density," Phys. Rev. Appl. **17**, 014018 (2022).

[4]J. Halbritter, "Comparison between measured and calculated RF losses in the superconducting state," Z. Phys. **238**, 466–476 (1970).

[5]A. Gurevich, "Theory of RF superconductivity for resonant cavities," Supercond. Sci. Technol. **30**, 034004 (2017).

[6]T. Kubo and A. Gurevich, "Field-dependent nonlinear surface resistance and its optimization by surface nanostructuring in superconductors," Phys. Rev. B **100**, 064522 (2019).

[7]A. Gurevich and T. Kubo, "Surface impedance and optimum surface resistance of a superconductor with an imperfect surface," Phys. Rev. B **96**, 184515 (2017).

[8]A. Grassellino, A. Romanenko, D. Sergatskov, O. Melnychuk, Y. Trenikhina, A. Crawford, A. Rowe, M. Wong, T. Khabiboulline, and F. Barkov, "Nitrogen and argon doping of niobium for superconducting radio frequency cavities: A pathway to highly efficient accelerating structures," Supercond. Sci. Technol. **26**, 102001 (2013).

[9]J. T. Maniscalco, D. Gonnella, and M. Liepe, "The importance of the electron mean free path for superconducting radio-frequency cavities," J. Appl. Phys. **121**, 043910 (2017).

[10]W. D. Oliver and P. B. Welander, "Materials in superconducting quantum bits," MRS Bull. **38**, 816–825 (2013).

[11]J. Zmuidzinas, "Superconducting microresonators: Physics and applications," Annu. Rev. Condens. Matter Phys. **3**, 169–214 (2012).

[12]H. S. Padamsee, "Superconducting radio-frequency cavities," Annu. Rev. Nucl. Part. Sci. **64**, 175–196 (2014).

[13]C. W. Leemann, D. R. Douglas, and G. A. Krafft, "The continuous electron beam accelerator facility: CEBAF at the Jefferson laboratory," Annu. Rev. Nucl. Part. Sci. **51**, 413–450 (2001).

[14]J. Rossbach, "A VUV free electron laser at the TESLA test facility at DESY," Nucl. Instrum. Methods Phys. Res. Sect. A: Accel. Spectrom. Detect. Assoc. Equip. **375**, 269–273 (1996), Proceedings of the 17th International Free Electron Laser Conference.

[15]C. Bostedt, S. Boutet, D. M. Fritz, Z. Huang, H. J. Lee, H. T. Lemke, A. Robert, W. F. Schlotter, J. J. Turner, and G. J. Williams, "Linac coherent light source: The first five years," Rev. Mod. Phys. **88**, 015007 (2016).

[16]M. Altarelli, R. Brinkmann, and M. Chergui, "The european x-ray free-electron laser. Technical design report," Tech. Rep. (DESY, 2007).

[17]S. Henderson, W. Abraham, A. Aleksandrov, C. Allen, J. Alonso, D. Anderson, D. Arenius, T. Arthur, S. Assadi, J. Ayers, and P. Bach, "The spallation neutron source accelerator system design," Nucl. Instrum. Methods Phys. Res. Sect. A: Accel. Spectrom. Detect. Assoc. Equip. **763**, 610–673 (2014).

[18]G. Bollen, "FRIB—Facility for rare isotope beams," AIP Conf. Proc. **1224**, 432–441 (2010).

[19]V. Lebedev, "The PIP-II reference design report," Tech. Rep. (Fermi National Accelerator Lab, 2015).

[20]M. Lindroos, S. Bousson, R. Calaga, H. Danared, G. Devanz, R. Duperrier, J. Eguia, M. Eshraqi, S. Gammino, H. Hahn, and A. Jansson, "The European spallation source," Nucl. Instrum. Methods Phys. Res. Sect. B: Beam Interact. Mater. Atoms **269**, 3258–3260 (2011), Proceedings of the 10th European Conference on Accelerators in Applied Research and Technology (ECAART10).

[21]D. Jeon, I.-S. Hong, H. J. Kim, J. W. Kim, R. Bodenstein, H. J. Cha, S.-J. Choi, S. Choi, O. Choi, H. Do, and B. H. Choi, "Design of the RAON accelerator systems," J. Korean Phys. Soc. **65**, 1010–1019 (2014).

[22]N. Phinney, N. Toge, and N. Walker, 'ILC reference design report volume 3-accelerator," arXiv:0712.2361 (2007).

[23]C. E. Reece, "Continuous wave superconducting radio frequency electron linac for nuclear physics research," Phys. Rev. Accel. Beams **19**, 124801 (2016).

[24]D. Gonnella, R. Eichhorn, F. Furuta, M. Ge, D. Hall, V. Ho, G. Hoffstaetter, M. Liepe, T. O'Connell, S. Posen, P. Quigley, J. Sears, V. Veshcherevich, A. Grassellino, A. Romanenko, and D. A. Sergatskov, "Nitrogen-doped 9-cell cavity performance in a test cryomodule for LCLS-IIa)," J. Appl. Phys. **117**, 023908 (2015).

[25]P. Dhakal, "Nitrogen doping and infusion in SRF cavities: A review," Phys. Open **5**, 100034 (2020).

[26]P. Dhakal, G. Ciovati, G. R. Myneni, K. E. Gray, N. Groll, P. Maheshwari, D. M. McRae, R. Pike, T. Proslier, F. Stevie, R. P. Walsh, Q. Yang, and J. Zasadzinzki, "Effect of high temperature heat treatments on the quality factor of a large-grain superconducting radio-frequency niobium cavity," Phys. Rev. ST Accel. Beams **16**, 042001 (2013).

[27]G. Ciovati, P. Dhakal, and A. Gurevich, "Decrease of the surface resistance in superconducting niobium resonator cavities by the microwave field," Appl. Phys. Lett. **104**, 092601 (2014), https://pubs.aip.org/aip/apl/article-pdf/doi/10.1063/1.4867339/13170033/092601_1_online.pdf.

[28]G. Ciovati, P. Dhakal, and G. R. Myneni, "Superconducting radio-frequency cavities made from medium and low-purity niobium ingots," Supercond. Sci. Technol. **29**, 064002 (2016).

[29]D. Gonnella, S. Aderhold, A. Burrill, E. Daly, K. Davis, A. Grassellino, C. Grimm, T. Khabiboulline, F. Marhauser, O. Melnychuk, A. Palczewski, S. Posen, M. Ross, D. Sergatskov, A. Sukhanov, Y. Trenikhina, and K. Wilson, "Industrialization of the nitrogen-doping preparation for SRF cavities for LCLS-II," Nucl. Instrum. Methods Phys. Res. Sect. A: Accel. Spectrom. Detect. Assoc. Equip. **883**, 143–150 (2018).

[30]D. Gonnella, S. Aderhold, D. Bafia, A. Burrill, M. Checchin, M. Ge, A. Grassellino, G. Hays, M. Liepe, M. Martinello, A. Palczewski, S. Posen, T. Raubenheimer, C. Reece, A. Romanenko, and M. Ross, "The LCLS-II he high q and gradient R&D program," in *Conference proceeding: 19th International Conference on RF Superconductivity*, (JACoW Publishing, Geneva, 2019)

[31]E. M. Lechner, J. W. Angle, F. A. Stevie, M. J. Kelley, C. E. Reece, and A. D. Palczewski, "RF surface resistance tuning of superconducting niobium via thermal diffusion of native oxide," Appl. Phys. Lett. **119**, 082601 (2021); A. D. Palczewski, E. M. Lechner, and C. E. Reece. "Methods of controllable interstitial oxygen doping in niobium," U.S. Patent No. 11,920,253. 5 Mar. 2024. https://patents.google.com/patent/US11920253B2/en.

[32]S. Posen, A. Romanenko, A. Grassellino, O. Melnychuk, and D. Sergatskov, "Ultralow surface resistance via vacuum heat treatment of superconducting radio-frequency cavities," Phys. Rev. Appl. **13**, 014024 (2020).

[33]H. Ito, H. Araki, K. Takahashi, and K. Umemori, "Influence of furnace baking on Q–E behavior of superconducting accelerating cavities," Prog. Theor. Exp. Phys. **2021**, 071G01.

[34]R. W. Powers and M. V. Doyle, "Diffusion of interstitial solutes in the group V transition metals," J. Appl. Phys. **30**, 514–524 (1959).
[35]W. DeSorbo, "Effect of dissolved gases on some superconducting properties of niobium," Phys. Rev. **132**, 107–121 (1963).
[36]C. C. Koch, J. O. Scarbrough, and D. M. Kroeger, "Effects of interstitial oxygen on the superconductivity of niobium," Phys. Rev. B **9**, 888–897 (1974).
[37]B. Goodman and G. Kuhn, "Influence des défauts étendus sur les propriétés supraconductrices du niobium," J. Phys. **29**, 240–252 (1968).
[38]J. Kirschenbaum, "Superconducting critical fields in niobium and niobium containing oxygen," Phys. Rev. B **12**, 3690–3696 (1975).
[39]D. C. Ford, L. D. Cooley, and D. N. Seidman, "First-principles calculations of niobium hydride formation in superconducting radio-frequency cavities," Supercond. Sci. Technol. **26**, 095002 (2013).
[40]F. Barkov, A. Romanenko, and A. Grassellino, "Direct observation of hydrides formation in cavity-grade niobium," Phys. Rev. ST Accel. Beams **15**, 122001 (2012).
[41]D. C. Ford, L. D. Cooley, and D. N. Seidman, "Suppression of hydride precipitates in niobium superconducting radio-frequency cavities," Supercond. Sci. Technol. **26**, 105003 (2013).
[42]G. Ciovati, "Improved oxygen diffusion model to explain the effect of low-temperature baking on high field losses in niobium superconducting cavities," Appl. Phys. Lett. **89**, 022507 (2006).
[43]P. Prieto, L. Galan, J. M. Sanz, and F. Rueda, "An XPS study of the kinetics of dissolution of ZrO_2 in α-Zr," Surf. Interface Anal. **16**, 535–539 (1990).
[44]J. Giber and H. Oechsner, "Dissolution of anodic Ta_2O_5 layers into polycrystalline tantalum," Thin Solid Films **131**, 279–287 (1985).
[45]A. P. Place, L. V. Rodgers, P. Mundada, B. M. Smitham, M. Fitzpatrick, Z. Leng, A. Premkumar, J. Bryon, A. Vrajitoarea, S. Sussman, and G. Cheng, "New material platform for superconducting transmon qubits with coherence times exceeding 0.3 milliseconds," Nat. Commun. **12**, 1779 (2021).
[46]C. Wang, X. Li, H. Xu, Z. Li, J. Wang, Z. Yang, Z. Mi, X. Liang, T. Su, C. Yang, and G. Wang, "Towards practical quantum computers: Transmon qubit with a lifetime approaching 0.5 milliseconds," npj Quantum Inf. **8**, 3 (2022).
[47]C. P. Bean and J. D. Livingston, "Surface barrier in type-II superconductors," Phys. Rev. Lett. **12**, 14–16 (1964).
[48]A. Gurevich and G. Ciovati, "Dynamics of vortex penetration, jumpwise instabilities, and nonlinear surface resistance of type-II superconductors in strong RF fields," Phys. Rev. B **77**, 104501 (2008).
[49]A. Gurevich, "Superconducting radio-frequency fundamentals for particle accelerators," Rev. Accel. Sci. Technol. **5**, 119–146 (2012).
[50]W. Pathirana and A. Gurevich, "Superheating field in superconductors with nanostructured surfaces," Front. Electron. Mater. **3**, 1246016 (2023).
[51]T. Kubo, "Multilayer coating for higher accelerating fields in superconducting radio-frequency cavities: A review of theoretical aspects," Supercond. Sci. Technol. **30**, 023001 (2016).
[52]J. W. Angle, A. D. Palczewski, C. E. Reece, F. A. Stevie, and M. J. Kelley, "Advances in secondary ion mass spectrometry for N-doped niobium," J. Vac. Sci. Technol. B **39**, 024004 (2021), https://pubs.aip.org/avs/jvb/article-pdf/doi/10.1116/6.0000848/13302089/024004_1_online.pdf.
[53]J. W. Angle, E. M. Lechner, A. D. Palczewski, C. E. Reece, F. A. Stevie, and M. J. Kelley, "Improved quantitation of SIMS depth profile measurements of niobium via sample holder design improvements and characterization of grain orientation effects," J. Vac. Sci. Technol. B **40**, 024003 (2022).
[54]H. Oechsner, J. Giber, H. Füßer, and A. Darlinski, "Phase transition and oxide dissolution processes in vacuum-annealed anodic Nb_2O_5/Nb systems," Thin Solid Films **124**, 199–210 (1985).
[55]B. King, H. Patel, D. Gulino, and B. Tatarchuk, "Kinetic measurements of oxygen dissolution into niobium substrates: In situ x-ray photoelectron spectroscopy studies," Thin Solid Films **192**, 351–369 (1990).
[56]J. Crank, *The Mathematics of Diffusion* (Oxford University Press, 1979).
[57]M. Delheusy, A. Stierle, N. Kasper, R. P. Kurta, A. Vlad, H. Dosch, C. Antoine, A. Resta, E. Lundgren, and J. Andersen, "X-ray investigation of subsurface interstitial oxygen at Nb/oxide interfaces," Appl. Phys. Lett. **92**, 101911 (2008).
[58]G. D. L. Semione, A. D. Pandey, S. Tober, J. Pfrommer, A. Poulain, J. Drnec, G. Schütz, T. F. Keller, H. Noei, V. Vonk, B. Foster, and A. Stierle, "Niobium near-surface composition during nitrogen infusion relevant for superconducting radio-frequency cavities," Phys. Rev. Accel. Beams **22**, 103102 (2019).
[59]F. Boratto and R. Reed-Hill, "On the calculations of the diffusion coefficients of oxygen and nitrogen in niobium," Metall. Trans. A **8**, 1233–1238 (1977).
[60]R. Gibala and C. Wert, "The clustering of oxygen in solid solution in niobium—I. Experimental," Acta Metall. **14**, 1095–1103 (1966).
[61]C. Ang, "Activation energies and diffusion coefficients of oxygen and nitrogen in niobium and tantalum," Acta Metall. **1**, 123–125 (1953).
[62]R. Kirchheim, "Metals as sinks and barriers for interstitial diffusion with examples for oxygen diffusion in copper, niobium and tantalum," Acta Metall. **27**, 869–878 (1979).
[63]K. Reddy and A. Cooper, "Oxygen diffusion in MgO and α-Fe_2O_3," J. Am. Ceram. Soc. **66**, 664–666 (1983), https://ceramics.onlinelibrary.wiley.com/doi/pdf/10.1111/j.1151-2916.1983.tb10618.x.
[64]C. Cantoni, D. K. Christen, M. Varela, J. R. Thompson, S. J. Pennycook, E. D. Specht, and A. Goyal, "Deposition and characterization of $YBa_2Cu_3O_7$-δ/$LaMnO_3$/MgO/TiN heterostructures on cu metal substrates for development of coated conductors," J. Mater. Res. **18**, 2387–2400 (2003).
[65]V. Gusakov, "Unified model of diffusion of interstitial oxygen in silicon and germanium crystals," J. Phys.: Condens. Matter **17**, S2285 (2005).
[66]R. Nakamura, T. Toda, S. Tsukui, M. Tane, M. Ishimaru, T. Suzuki, and H. Nakajima, "Diffusion of oxygen in amorphous Al_2O_3, Ta_2O_5, and Nb_2O_5," J. Appl. Phys. **116**, 033504 (2014), https://pubs.aip.org/aip/jap/article-pdf/doi/10.1063/1.4889800/15139262/033504_1_online.pdf.
[67]W. M. Yim, E. J. Stofko, P. J. Zanzucchi, J. I. Pankove, M. Ettenberg, and S. L. Gilbert, "Epitaxially grown AlN and its optical band gap," J. Appl. Phys. **44**, 292–296 (2003).
[68]M. Sterntzke and G. Müller, "Eels study of oxygen diffusion in aluminum nitride," J. Am. Ceram. Soc. **77**, 737–742 (1994).
[69]C. Ozgit, I. Donmez, M. Alevli, and N. Biyikli, "Self-limiting low-temperature growth of crystalline aln thin films by plasma-enhanced atomic layer deposition," Thin Solid Films **520**, 2750–2755 (2012).
[70]H. Martens, H. Diepers, and R. Sun, "Improvement of superconducting Nb cavities by anodic oxide films," Phys. Lett. A **34**, 439–440 (1971).
[71]M. B. Gomes, S. Onofre, S. Juanto, and L. D. S. Bulhões, "Anodization of niobium in sulphuric acid media," J. Appl. Electrochem. **21**, 1023–1026 (1991).
[72]M. Hatano, T. Nishino, and U. Kawabe, "Effects of thermal annealing on superconducting Nb and NbN films," J. Vac. Sci. Technol. A **6**, 2381–2385 (1988).
[73]M. Checchin and A. Grassellino, "High-field Q-slope mitigation due to impurity profile in superconducting radio-frequency cavities," Appl. Phys. Lett. **117**, 032601 (2020).
[74]Z. Yang, J. Hao, S. Quan, L. Lin, F. Wang, F. Jiao, and K. Liu, "Effective medium temperature baking of 1.3 GHz single cell SRF cavities," Physica C **599**, 1354092 (2022).
[75]G. Ciovati, "Effect of low-temperature baking on the radio-frequency properties of niobium superconducting cavities for particle accelerators," J. Appl. Phys. **96**, 1591–1600 (2004).
[76]G. Eremeev and H. Padamsee, "Change in high field Q-slope by baking and anodizing," Physica C **441**, 62–65 (2006), Proceedings of the 12th International Workshop on RF Superconductivity.
[77]G. Ciovati, P. Kneisel, and A. Gurevich, "Measurement of the high-field Q drop in a high-purity large-grain niobium cavity for different oxidation processes," Phys. Rev. ST Accel. Beams **10**, 062002 (2007).
[78]A. Romanenko, A. Grassellino, F. Barkov, and J. P. Ozelis, "Effect of mild baking on superconducting niobium cavities investigated by sequential nanoremoval," Phys. Rev. ST Accel. Beams **16**, 012001 (2013).
[79]R. M. McFadden, M. Asaduzzaman, and T. Junginger, "Comment on 'Strong Meissner screening change in superconducting radio frequency cavities due to mild baking' [Appl. Phys. Lett. **104**, 072601 (2014)]," arXiv:2305.02129 (2023).

[80]A. Romanenko, A. Grassellino, F. Barkov, A. Suter, Z. Salman, and T. Prokscha, "Strong Meissner screening change in superconducting radio frequency cavities due to mild baking," Appl. Phys. Lett. **104**, 072601 (2014).
[81]C. Benvenuti, S. Calatroni, P. Darriulat, M. Peck, A.-M. Valente, and C. Hof, "Study of the residual surface resistance of niobium films at 1.5 GHz," Physica C **351**, 421–428 (2001).
[82]B. Visentin, "3.8 low, medium, high field Q-slopes change with surface treatments," Beam Dynam. Newslett. 39, 94 (2006).
[83]H. Safa, "High field behavior of SCRF cavities," in *Proceedings of the 10th Workshop on RF Superconductivity, Tsukuba, Japan* (Citeseer, 2001).
[84]F. London and H. London, "The electromagnetic equations of the supraconductor," Proc. R. Soc. London. Ser. A-Math. Phys. Sci. **149**, 71–88 (1935).
[85]R. W. Simon and P. M. Chaikin, "Josephson tunneling studies of magnetic screening in proximity-superconducting silver," Phys. Rev. B **23**, 4463–4469 (1981).
[86]P. Koufalis, D. Hall, M. Liepe, and J. Maniscalco, "Effects of interstitial oxygen and carbon on niobium superconducting cavities," arXiv:1612.08291 (2016).
[87]K. K. Schulze, "Preparation and characterization of ultra-high-purity niobium," JOM **33**, 33–41 (1981).
[88]M. Tinkham, "Penetration depth, susceptibility, and nuclear magnetic resonance in finely divided superconductors," Phys. Rev. **110**, 26–29 (1958).
[89]B. W. Maxfield and W. L. McLean, "Superconducting penetration depth of niobium," Phys. Rev. **139**, A1515–A1522 (1965).
[90]V. L. Ginzburg, V. L. Ginzburg, and L. Landau, *On the Theory of Superconductivity* (Springer, 2009).
[91]G. Ciovati, "Review of the frontier workshop and Q-slope results," Physica C **441**, 44–50 (2006), Proceedings of the 12th International Workshop on RF Superconductivity.
[92]B. Visentin, Y. Gasser, M. Bruchon, F. Eozenou, and J. Charrier, "Optimization of baking parameters for electropolished niobium superconducting cavities," in *13th Workshop on RF Superconductors, Beijing, China* (JACoW Publishing, Geneva,, 2007).
[93]P. Bauer, G. Ciovati, H. Edwards, J. Halbritter, K. Saito, and B. Visentin, "A collection of selected high field Q-slope studies, models and comments," Review of Q-drop in SRF cavities , 05–56 (2006).
[94]B. Visentin, Y. Gasser, and J. Charrier, "First results on fast baking," Physica C **441**, 66–69 (2006), Proceedings of the 12th International Workshop on RF Superconductivity.
[95]G. Eremeev and H. Padamsee, "Temperature mapping results on the high-field Q-slope of 1500 MHz single cell superconducting radiofrequency cavities baked in-situ at 400 C," in *2007 IEEE Particle Accelerator Conference (PAC)* (IEEE, 2007), pp. 2334–2336.
[96]D. Bafia, A. Grassellino, and A. Romanenko, "The role of oxygen concentration in enabling high gradients in niobium SRF cavities," Tech. Rep. (Fermi National Accelerator Lab.(FNAL), Batavia, IL (United States), 2021).
[97]C. Benvenuti, S. Calatroni, and V. Ruzinov, "Diffusion of oxygen in niobium during bake-out," in *Proceedings of the 10th Workshop on RF Superconductivity* (JACoW Publishing, Geneva, 2001), pp. 441.
[98]B. Aune, R. Bandelmann, D. Bloess, B. Bonin, A. Bosotti, M. Champion, C. Crawford, G. Deppe, B. Dwersteg, D. A. Edwards, and H. T. Edwards, "Superconducting TESLA cavities," Phys. Rev. ST Accel. Beams **3**, 092001 (2000).
[99]G. Catelani and J. P. Sethna, "Temperature dependence of the superheating field for superconductors in the high-κ london limit," Phys. Rev. B **78**, 224509 (2008).
[100]M. K. Transtrum, G. Catelani, and J. P. Sethna, "Superheating field of superconductors within Ginzburg-Landau theory," Phys. Rev. B **83**, 094505 (2011).
[101]T. Kubo, "Field limit and nano-scale surface topography of superconducting radio-frequency cavity made of extreme type II superconductor," Prog. Theor. Exp. Phys. **2015**, 063G01.
[102]E. M. Lechner, J. W. Angle, C. Baxley, M. J. Kelley, and C. E. Reece, "Topographic evolution of heat-treated nb upon electropolishing for superconducting RF applications," Phys. Rev. Accel. Beams **26**, 103101 (2023).
[103]T. Kubo, "Magnetic field enhancement at a pit on the surface of a superconducting accelerating cavity," Prog. Theor. Exp. Phys. **2015**, 073G01 (2015).
[104]J. Knobloch, R. Geng, M. Liepe, and H. Padamsee, "High-field Q slope in superconducting cavities due to magnetic field enhancement at grain boundaries," in *Proceedings of the 9th Workshop on RF Superconductivity* (Citeseer, 1999), pp. 77–91.
[105]Y. Xie, M. Liepe, and H. Padamsee, "Quench simulation using a ring-type defect model," in *Conference proceeding: 15th International Conference on RF Superconductivity* (JACoW Publishing, Geneva, 2011).
[106]C. Xu, C. E. Reece, and M. J. Kelley, "Simulation of nonlinear superconducting RF losses derived from characteristic topography of etched and electropolished niobium surfaces," Phys. Rev. Accel. Beams **19**, 033501 (2016).
[107]E. M. Lechner, B. D. Oli, J. Makita, G. Ciovati, A. Gurevich, and M. Iavarone, "Characterization of dissipative regions of a N-doped superconducting radio-frequency cavity," Front. Electron. Mater. **3**, 1235918 (2023).
[108]N. Sitaraman, T. Arias, A. Harbick, M. Liepe, and M. Transtrum, "A comprehensive picture of hydride formation and dissipation," in *Proceedings of 21st International Conference on RF Superconductors (SRF'23)* (JACoW Publishing, Geneva, 2023), pp. 119–123.
[109]E. M. Lechner, B. D. Oli, J. Makita, G. Ciovati, A. Gurevich, and M. Iavarone, "Electron tunneling and X-ray photoelectron spectroscopy studies of the superconducting properties of nitrogen-doped niobium resonator cavities," Phys. Rev. Appl. **13**, 044044 (2020).